PAPER • OPEN ACCESS

Overview of the TJ-II stellarator research programme towards model validation in fusion plasmas

To cite this article: C. Hidalgo *et al* 2022 *Nucl. Fusion* **62** 042025

OPEN ACCESS
IOP Publishing | International Atomic Energy Agency Nuclear Fusion
Nucl. Fusion **62** (2022) 042025 (14pp) https://doi.org/10.1088/1741-4326/ac2ca1

Overview of the TJ-II stellarator research programme towards model validation in fusion plasmas

C. Hidalgo[1,*], E. Ascasíbar[1], D. Alegre[1], A. Alonso[1], J. Alonso[1], R. Antón[1], A. Baciero[1], J. Baldzuhn[2], J.M. Barcala[3], L. Barrera[1], E. Blanco[1], J. Botija[1], L. Bueno[1], S. Cabrera[1], A. de Castro[1], E. de la Cal[1], I. Calvo[1], A. Cappa[1], D. Carralero[1], R. Carrasco[1], B. Carreras[4], R. Castro[1], A. de Castro[1], L. Cebrián[1], A.A. Chmyga[5], M. Chamorro[1], P. Colino[1], F. de Aragón[1], M. Drabinskiy[6], J. Duque[1], L. Eliseev[6], F.J. Escoto[1], T. Estrada[1], M. Ezzat[1], F. Fraguas[1], D. Fernández-Ruiz[1], J.M. Fontdecaba[1], A. Gabriel[1], D. Gadariya[1], L. García[4], I. García-Cortés[1], R. García-Gómez[1], J.M. García-Regaña[1], A. González-Jerez[1], G. Grenfell[7], J. Guasp[1], V. Guisse[1], J. Hernández-Sánchez[1], J. Hernanz[1], A. Jiménez-Denche[1], P. Khabanov[6], N. Kharchev[8], R. Kleiber[2], F. Koechl[2], T. Kobayashi[9], G. Kocsis[10], M. Koepke[11], A.S. Kozachek[5], L. Krupnik[5], F. Lapayese[1], M. Liniers[1], B. Liu[12], D. López-Bruna[1], B. López-Miranda[1], U. Losada[1], E. de la Luna[1], S.E. Lysenko[6], F. Martín-Díaz[1], G. Martín-Gómez[1], E. Maragkoudakis[1], J. Martínez-Fernández[1], K.J. McCarthy[1], F. Medina[1], M. Medrano[1], A.V. Melnikov[6,13], P. Méndez[1], F.J. Miguel[1], B. van Milligen[1], A. Molinero[3], G. Motojima[9], S. Mulas[1], Y. Narushima[9], M. Navarro[1], I. Nedzelskiy[14], R. Nuñez[1], M. Ochando[1], S. Ohshima[15], E. Oyarzábal[1], J.L. de Pablos[1], F. Palomares[1], N. Panadero[1], F. Papoušek[1], F. Parra[16], C. Pastor[1], I. Pastor[1], A. de la Peña[1], R. Peralta[1], A. Pereira[1], P. Pons-Villalonga[1], H. Polaino[1], A.B. Portas[1], E. Poveda[1], F.J. Ramos[1], G.A. Rattá[1], M. Redondo[1], C. Reynoso[1], E. Rincón[1], C. Rodríguez-Fernández[1], L. Rodríguez-Rodrigo[1], A. Ros[1], E. Sánchez[1], J. Sánchez[1], E. Sánchez-Sarabia[1], S. Satake[9], J.A. Sebastián[1], R. Sharma[14], N. Smith[17], C. Silva[14], E.R. Solano[1], A. Soleto[1], M. Spolaore[18], T. Szepesi[10], F.L. Tabarés[1], D. Tafalla[1], H. Takahashi[9], N. Tamura[9], H. Thienpondt[1], A. Tolkachev[1], R. Unamuno[1], J. Varela[4], J. Vega[1], J.L. Velasco[1], I. Voldiner[1], S. Yamamoto[15] and the TJ-II Team[1]

[1] Laboratorio Nacional de Fusión, CIEMAT, Madrid, Spain
[2] Max-Planck-Institut für Plasmaphysik, Greifswald, Germany
[3] Department of Technology, CIEMAT, Madrid, Spain
[4] Universidad Carlos III, Madrid, Spain
[5] Institute of Plasma Physics, NSC KIPT Kharkov, Ukraine
[6] National Research Centre 'Kurchatov Institute', Moscow, Russian Federation
[7] Max-Planck-Institut für Plasmaphysik, Garching, Germany
[8] General Physics Institute, Russian Academy of Sciences, Moscow, Russian Federation
[9] National Institute for Fusion Science, Toki, Japan

[*] Author to whom any correspondence should be addressed.

[10] Centre for Energy Research, Budapest, Hungary
[11] Department of Physics and Astronomy, West Virginia University, United States of America
[12] ENN Energy Research Institute, Langfang, Hebei, China
[13] National Research Nuclear University 'MEPhI', Moscow, Russian Federation
[14] IPFN, Instituto Superior Técnico, Universidade de Lisboa, Lisboa, Portugal
[15] Institute of Advanced Energy, Kyoto University, Uji, Japan
[16] Rudolf Peierls Centre for Theoretical Physics, University of Oxford, United Kingdom
[17] Eindhoven University of Technology, Netherlands
[18] Consorzio RFX (CNR, ENEA, INFN, Università di Padova, Acciaierie Venete SpA), Padova, Italy

E-mail: carlos.hidalgo@ciemat.es

Received 9 June 2021, revised 23 September 2021
Accepted for publication 4 October 2021
Published 14 April 2022

Abstract

TJ-II stellarator results on modelling and validation of plasma flow asymmetries due to on-surface potential variations, plasma fuelling physics, Alfvén eigenmodes (AEs) control and stability, the interplay between turbulence and neoclassical (NC) mechanisms and liquid metals are reported. Regarding the validation of the neoclassically predicted potential asymmetries, its impact on the radial electric field along the flux surface has been successfully validated against Doppler reflectometry measurements. Research on the physics and modelling of plasma core fuelling with pellets and tracer encapsulated solid pellet injection has shown that, although post-injection particle radial redistributions can be understood qualitatively from NC mechanisms, turbulence and fluctuations are strongly affected during the ablation process. Advanced analysis tools based on transfer entropy have shown that radial electric fields do not only affect the radial turbulence correlation length but are also capable of reducing the propagation of turbulence from the edge into the scrape-off layer. Direct experimental observation of long range correlated structures show that zonal flow structures are ubiquitous in the whole plasma cross-section in the TJ-II stellarator. Alfvénic activity control strategies using ECRH and ECCD as well as the relation between zonal structures and AEs are reported. Finally, the behaviour of liquid metals exposed to hot and cold plasmas in a capillary porous system container was investigated.

Keywords: stellarator, transport, plasma

(Some figures may appear in colour only in the online journal)

1. Introduction

Plasma physics and fusion technology issues have been successfully developed in previous years, with present-day experiments being only a generation away from fusion reactor plasma conditions. However, the extrapolation of current experiments to reactor devices cannot be based exclusively on an empirical approach. Therefore, a significant effort must be devoted to model validation against experiments.

Using its unique flexibility and advanced plasma diagnostics, the TJ-II stellarator is contributing to the understanding of critical plasma physics challenges in fusion plasmas. TJ-II is a heliac type device (major radius 1.5 m, minor radius $\leqslant 0.22$ m, four periods, average magnetic field on axis 0.95 T, plasma volume $\leqslant 1$ m^3). Both ECRH (two gyrotrons, 53.2 GHz, $P \leqslant 300$ kW each, suitable for X2 heating) and neutral beam heating (NBI) heating (two H_0 injectors, $E \leqslant 30$ kV, $P \leqslant 600$ kW each) can be used to produce and sustain the discharge.

Concerning specific physics areas of research, work at TJ-II has been focussed on:

Transport and confinement. The demonstration of good confinement at reactor-relevant conditions in an optimised configuration is central to the assessment of the stellarator reactor line. This requires not only confirming the reduction and validation of neoclassical (NC) transport in optimised stellarators but also to understand and control turbulent transport. Furthermore, the accumulation of high-Z impurities in the core is a long-standing concern in the stellarator community that makes the control of transport of impurities crucial.

Particle fuelling and neutral dynamics. An important factor contributing to the particle transport is the density gradient localization, which is closely connected to neutral refuelling. Fuelling of core plasma is foreseen by pellet systems that inject particles at high speed deep into the plasma. However, at

reactor relevant parameters, pellets would be unable to reach the core plasma region. Therefore it is mandatory to quantify the importance of both NC and turbulent mechanisms in the foreseen level of inward particle transport.

Magneto-hydrodynamic (*MHD*) *stability and fast particle physics.* MHD stability need to be assessed both from experimental and theoretical standpoints. Additionally, fast ion-driven Alfvénic instabilities must be characterised and modelled in view of alpha particle transport in reactor scenarios. While most of previous research has been focussed on the excitation and impact of fast ion modes in plasma performance, there is a growing interest in the impact on fast particles of turbulence and self-organization phenomena.

Plasma edge physics. Scrape-off layer (SOL) transport in tokamaks is thought to be dominated by convective cells (filaments). However, it is an open question how the complex stellarator geometry of a non-axially symmetric SOL influences these structures. Clarifying whether the SOL width is dominated by local effects in the SOL region or/and by transport driven in the plasma edge is a relevant question for predicting power exhaust.

Plasma–wall interaction. Plasma wall conditions are key for good plasma performance. Schemes for wall conditioning and understanding of long-pulse behaviour of the plasma wall is essential for the development of reactor scenarios. The 'Laboratorio Nacional de Fusión' (LNF) addresses power exhaust physics by means of liquid metal studies. Recently, a facility for the optimization of liquid targets (OLMAT) has been built and installed, guaranteeing its compatibility with TJ-II plasma operation.

Next, we highlight some of the most relevant recent results in the framework of the TJ-II research programme.

2. Towards the validation of gyrokinetic and neoclassical simulations

2.1. Plasma potential and turbulence poloidal asymmetries

The validation of gyrokinetic (GK) predictions of turbulent fluctuations and the electrostatic potential variations on the flux surface, φ_1, calculated by NC codes, have been the target of a series of dedicated experiments carried out in TJ-II. A systematic characterization of the wavenumber spectra of plasma density fluctuations has been carried out by Doppler reflectometry (DR), which allows scanning different poloidally separated regions on the same flux surface and investigate asymmetries of the studied quantities [1, 2]. The difference in the amplitude and the wave number spectrum at the different locations over the surface have been compared with global linear GK simulations performed with the code EUTERPE. In the framework of a long-standing effort for the validation of asymmetries in TJ-II [3, 4] the perpendicular rotation velocity of the fluctuations measured with DR has also been compared with NC EUTERPE calculations that predict, under some scenarios, moderate to strong variations of the radial electric field and, with it, of the $E_r \times B$ flow (figure 1). Predictions and experiments agree qualitatively regarding the radial dependence of

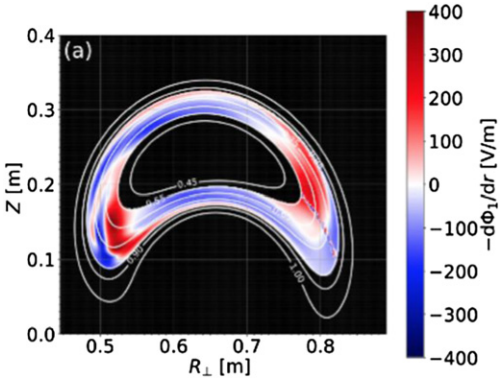

Figure 1. Predicted poloidal asymmetries of the radial electric field (E_r) due to the varying electrostatic potential over the surface. The variations are comparable to those found in the experiments by DR. Reproduced courtesy of IAEA. Figure from [1]. © EURATOM 2019.

the turbulence intensity, the turbulence dispersion relation and the correlation between the strength of the radial electric field variations and the rotation velocity of the fluctuations and how this depends on magnetic configuration. Recent experiments exploring configurations with different magnetic ripple have shown a reduction in the turbulence asymmetry in configurations with reduced ripple. In addition, the influence of base ion mass has been investigated in hydrogen and deuterium plasmas. The ion mass in TJ-II plasmas does not affect the properties of the turbulence, neither the amplitude nor the spectral shape or the poloidal asymmetry. GK simulations also do not show any dependence of the turbulence spectrum on the ion mass. Model validation will also benefit from the effort of verification of GK simulations in different computational domains [5] as well as from the application of the recently developed GK code Stella [6] to TJ-II, in particular, for the investigation of the turbulent transport of impurities [7].

Poloidal asymmetries in the radial electric field, E_r, are found that depend on the plasma collisionality. These results have been compared with the contribution to E_r arising from $-\varphi'_1$ as calculated with the NC version of the code EUTERPE. These results show variations in E_r comparable in size to those found in the experiments, but there is a disagreement regarding the sign of the E_r correction. Recent theoretical results [8] show that the effect of kinetic electrons on φ_1 has to be taken into account due to the strong T_e dependence of the electron contribution to φ_1 when the electrons are in the $1/\nu$ regime. These simulations can be performed with the newly developed NC code kinetic orbit-averaging solver for stellarators (KNOSOS) [9, 10]. KNOSOS is a freely available open-source code that provides a fast computation of low collisionality NC transport in sufficiently optimized three-dimensional magnetic confinement devices, by rigorously solving the bounce-averaged drift kinetic and quasineutrality equations derived in [2]. Where applicable, KNOSOS reproduces the results of the codes DKES and (the NC version of) EUTERPE and can be orders of magnitude faster than either of them. This means that KNOSOS can provide new figures of merit for stellarator optimization (apart from the

effective ripple) that could thus far not be included in optimization algorithms, such as the level of transport in the $\sqrt{\nu}$ regime (because its calculation was too slow with standard codes) or in the superbanana-plateau regime [because the tangential magnetic drift was not taken into account, see e.g. (figure 2)]. It can also greatly improve the speed and accuracy of predictive simulations. KNOSOS has been employed to compute the radial electric field of W7-X [11, 12]. It has also been coupled to the optimization suite STELLOPT [13] and has started to be employed in the design of new stellarator configurations.

2.2. Plasma fuelling and impurities

The continued exploitation of the combined cryogenic hydrogen and tracer encapsulated solid pellet (TESPEL) pellet injection system on TJ-II has provided new insight into pellet physics in stellarators and, in parallel, has permitted the benchmarking of a stellarator version of the pellet ablation and homogenization code HPI2 [14, 15] (figure 3). Experiments in TJ-II have shown that post-injection radial particle distributions can be understood qualitatively from NC predictions [15]. For instance, the large outward drift acceleration experienced by ablated pellet material results in low fuelling efficiencies (<25%) for injections from the outer plasma edge of this device. Indeed, tracer injections with polystyrene ($-C_8H_8-$) based TESPELs have confirmed an inverse mass dependence of the acceleration [16]. Additional experiments have also revealed that enhanced pellet ablation in the plasma core due to fast-electron impacts can lead to higher fuelling efficiencies as the outward drift acceleration is disrupted in the initial drift phase [17]. In particular, it is found that if a pellet is subject to excess ablation due to core fast electron impacts, the resultant pellet efficiency (deposited particles/delivered particles) increases by up to 50% with respect to injections into similar, fast-electron free, plasmas. More recently, comparisons between pellet experiments and HPI2 simulations have revealed that interactions between outward drifting pellet material and a resonant surface can lead to the abrupt deceleration of the outward drifting ablated pellet material and hence reduced pellet material loss [18]. The same experiments have shown that pellets can impact MHD plasma stability and broadband plasma turbulence strongly.

An important factor contributing to particle transport is the density gradient localization, which is closely connected to neutral refuelling in tokamak and stellarator devices. Plasma fuelling by systems that inject pellets deeply at high speed is foreseen for future reactors. However, at reactor relevant plasma densities and temperatures, pellets will not reach the core plasma region. This may result in density profiles with positive and negative density gradient regions. Therefore it is mandatory to quantify the importance of both NC and turbulent mechanisms on the foreseen level of inward and outward particle transport. Fluid and GK simulations have investigated the level of inward turbulent particle transport in the inverted density gradient region but comparisons of simulations with experimental fluctuation levels and fluxes are still missing. The stellarator TJ-II is well suited to investigate the influence of such positive and negative density gradients on plasma fluctuations and transport due to its unique capabilities to control plasma scenarios and magnetic configuration. Results show that plasma density fluctuations appear in both positive and negative density gradient regions in TJ-II plasmas, with normalized levels of density fluctuations that are higher in the negative density gradient region [19].

3. Towards the identification of Alfvén eigenmode actuators and core zonal flows

An ambitious research programme is in progress to investigate the relation between zonal structures and Alfvén eigenmodes (AEs) and its role in the nonlinear dynamics of AEs and transport as well as to develop and demonstrate AE control strategies using ECRH and ECCD in TJ-II.

3.1. Characterization and control of Alfvén eigenmodes

Controlling the amplitude of AEs in fusion plasmas is an open issue with essential relevance for ITER and beyond, because the fast ion losses associated with these modes might be deleterious for plasma performance and heating efficiency, as well as destructive for the plasma facing components. Destabilization of shear Alfvén waves depends on the precise magnetic configuration (rotational transform profile) and the balance between the fast particle drive and damping mechanisms. The impact of ECRH and ECCD has been investigated in stellarator devices [20] demonstrating a clear effect of ECCD on the observed mode spectrum (figure 4). For the case illustrated in the figure, adding counter-ECCD decreases the rotational transform in the core. Even though the total plasma current varies only by a small amount, the changes in the observed mode spectrum are clearly visible. Linear stability analysis using the FAR3d gyrofluid code has allowed for successful AE identification in different heating scenarios [21]. Such analysis needs, among other inputs, a calculation of the fast ion pressure and, since the experiments were not carried out with balanced NBI driven plasma current, an estimation of the NBCD becomes necessary. To this end TJ-II stellarator magnetic configurations and its NBI systems have been implemented in the Monte Carlo orbit following code ASCOT in order to determine the fast ion current. The electron response to this current, needed to calculate NBCD, has been obtained analytically by solving the drift kinetic equation for the electron distribution function interacting with NBI fast ions in the low collisionality limit [22]. Other sources of plasma current (i.e. bootstrap, ECCD) have also been estimated [21].

From the experimental point of view, a new helicoidal array of Mirnov coils, able to measure perturbations of the magnetic field in all directions, has been recently commissioned and will allow to determine the toroidal mode number (n) of the perturbations [23]. This set of probes will complement the already existing poloidal array, used to determine the poloidal mode number (m). It is expected that such enhancements in the theoretical/computational and experimental capabilities will significantly improve the interpretation of fast particle experiments. Operation scenarios combining fast ions from neutral

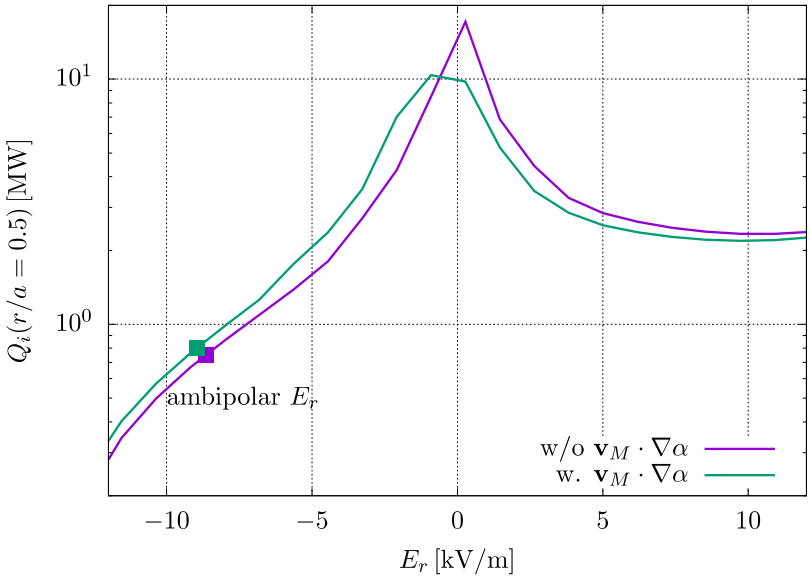

Figure 2. By including the tangential magnetic drift in the solution of the drift-kinetic equation (green line, to be compared with magenta line, calculated without this term) KNOSOS produces more accurate calculations of the NC energy flux for small values of the radial electric field, when the tangential magnetic drift is similar in size as the $E \times B$ drift. Reproduced with permission from [9].

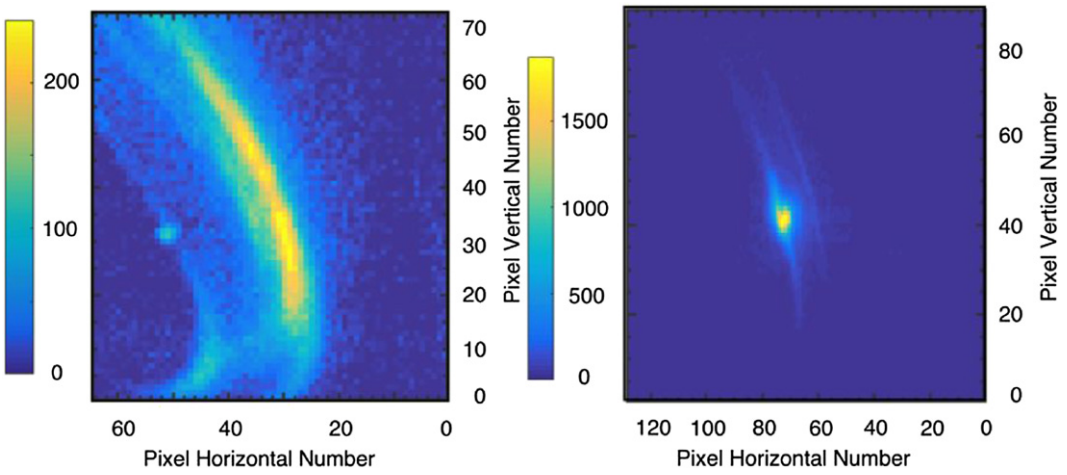

Figure 3. Despite much progress over the past decades, a complete comprehension of the physics processes involved in pellet ablation, pellet particle drift and diffusion is still outstanding. However, given the shared physics, comparative studies between both pellet types can provide new insight and understanding into physics processes and plasma response. Left: a single image obtained with a fast-frame imaging camera during the ablation of a 290 um diameter TESPEL containing aluminium tracer injected at 358 m s^{-1} into ECRH discharge #50443 confined using the standard 100_44_64 configuration. A C II transmission filter is used and the camera is set to 1 us exposure time and a frame rate of 525 kf s^{-1}. Right: a single image obtained during the ablation of a H_2 pellet injected at 950 m s^{-1} into ECRH discharge #50440 confined using the 100_44_64 configuration. No filter is used and the camera is set to 1 us exposure time and a frame rate of 350 kf s^{-1}. In both cases, the optical lens is located in a nearby tangential viewport and light is transferred to the camera using a coherent fibre bundle. Pellets are injected from right to left and colour bars represent light intensity. In the case of TESPEL and the C II filter, it is possible to capture images showing a fuller extent of the toroidal expansion and radial drift of its plasmoid clouds than is possible with H_2 pellets. This can provide new insights into the physics of pellet particle expansion and drift in TJ-II.

beam injection with variable activity of AEs using control actuators such as ECCD are the target for future experiments.

3.2. On the search of core zonal flows (ZFs) and the influence of Alfvén eigenmodes in the TJ-II stellarator

While most previous research efforts have been focussed on the excitation and impact of fast ion modes in plasma performance, because of the drain of energy related to fast particle losses with concomitant potential damages in the plasma facing components, there is a growing interest in the impact of fast particles on plasma turbulence and self-organization phenomena. Nonlinear electromagnetic stabilization by suprathermal pressure gradients has been found in GK simulations [24] providing an interpretation of the experimentally observed ion heat flux and stiffness reduction in the JET tokamak

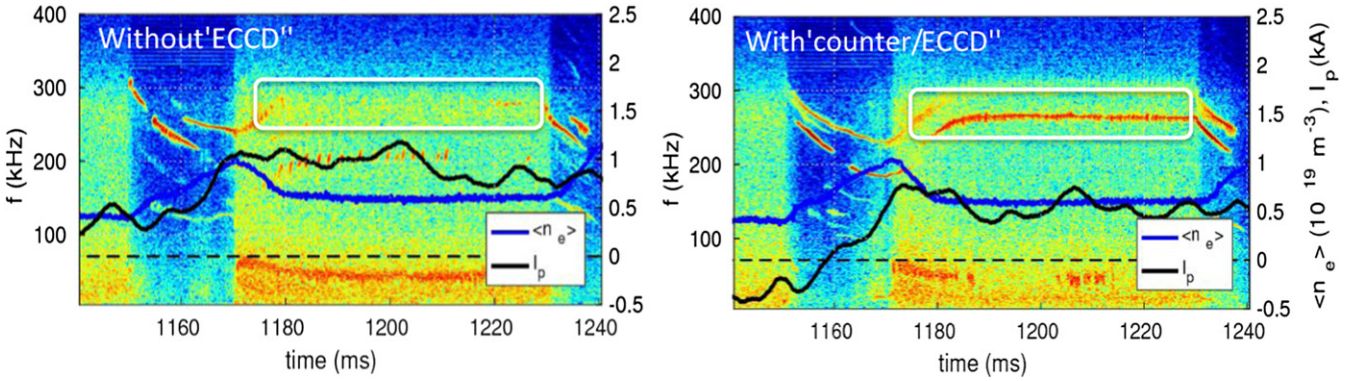

Figure 4. AEs actuators in TJ-II: (*a*) without ECCD (*b*) with on-axis counter-ECCD. The vacuum magnetic configuration modified by the different levels of plasma current and plasma parameters has been input to the FAR3d gyro-fluid code to study the linear evolution of AEs [21].

[25]. Understanding the underlying physics of this non-linear electromagnetic stabilization mechanism is an essential task for future fusion reactors where plasmas will be dominated by fast particle dynamics. The coexistence and interplay of fast ions with main instabilities such as ITG [26] and TEM [27] is an active area of research. In particular, non-linear excitations of zonal structures by fast particle driven modes have been predicted [28–30] but validation is still missing. The plasma scenarios where fast particle driven zonal structures would affect the nonlinear dynamics of AEs or/and turbulent transport is at present an active area of research.

The main focus of this work is the experimental search of ZFs and the possible influence of fast particle driven modes in the dynamics of ZFs in the plasma core region of fusion plasmas (figure 5). The results reported here have been drawn from a dedicated development based on a dual heavy ion beam probe (HIBP) system [31]. In this study both HIBP-I and HIBP-II systems were operated in scanning and fixed point mode to determine plasma profiles as well as plasma potential and density fluctuations at a specific radial location (figure 6). This unique set-up permits the simultaneous investigation of the radial structure of fluctuations, $E \times B$ driven transport [32] and long-range correlated scales in the whole plasma poloidal cross-section in the TJ-II stellarator. Plasma fluctuations are dominated by broadband turbulence in ECRH scenarios whereas in NBI regimes both broadband turbulence as well as Alfvénic instabilities are clearly detected. Previous experiments have shown that heating, magnetic configuration and plasma density scenarios affect the dynamics of AEs [33, 34].

Operating the HIBP in scanning mode from the high to the low field side allows determining the radial location of AEs. Depending of plasma conditions, AEs were radially localized deep in the core plasma ($\rho \approx 0.3$) or at mid-radius ($\rho \approx 0.6$) with frequencies in the range 100–400 kHz. Figure 7 shows a particular example of AEs localized near $\rho \approx 0.6$ with frequencies in the range 120–160 kHz (shot 49510). Mean plasma potential profiles have been investigated in NBI plasma regimes with different level of AE activity. Within uncertainties and in the explored plasma scenarios, mean plasma potential profiles are not significantly affected by the presence of AEs.

LRCs have been measured for plasma potential and density fluctuations during pure ECRH and combined ECRH + NBI plasma scenarios. The frequency resolved LRCs shown in figure 8 illustrate that LRCs only exist for plasma potential fluctuations, with phase shift close to zero, and not for density fluctuations. In regimes with Alfvenic instabilities, LRC are detected at AE frequencies and at low frequencies (<10 kHz). Therefore, these macro-structures, localized in the plasma core, are consistent low frequency ZFs, in agreement with the previous identification of ZFs in the plasma edge region [35].

Figure 9 shows the time evolution of LRCs measured for plasma potential fluctuations in the plasma core ($\rho \approx 0.6$) during pure ECRH and combined ECRH + NBI plasma scenarios (shot 49591). The plasma density evolves from $n \approx 0.6 \times 10^{19}$ m^{-3} (ECRH regime) up to $n \approx 0.8 \times 10^{19}$ m^{-3} (ECRH + NBI regime). It should be noted that there is a change in the sign of plasma potential from positive to negative values, reflecting a change in the mean radial electric field from electron root in the ECRH phase to the root in the ECRH + NBI phase [36]. LRCs in plasma potential exist with comparable levels in both ECRH and ECRH + NBI, reaching high values (coherence in the range of 0.8) for low frequency fluctuations (<10 kHz). Therefore, core LRCs are observed in a wide range of plasma scenarios.

Figure 10 shows the time evolution of LRCs measured for plasma potential fluctuations in the plasma core ($\rho \approx 0.3$) during pure ECRH and combined ECRH + NBI plasma scenarios (shot 49598). In these experiments the HIBP-I was in a fixed position ($\rho \approx 0.3$) whereas the HIBP-2 is in scanning mode exploring the limited plasma core region $\rho \approx 0.2$–0.4. The radial scanning of the HIBP-II system allows measuring the radial profile of the core plasma potential resulting in positive radial electric fields (i.e. electron root) with values in the range of 1 kV m^{-1}. The amplitude of the LRC is significantly affected by plasma density in the ECRH regime, as shown in figure 9 (shot 49591) where the density reaches values of $n \approx 0.6 \times 10^{19}$ m^{-3} to be compared with results shown in figure 10

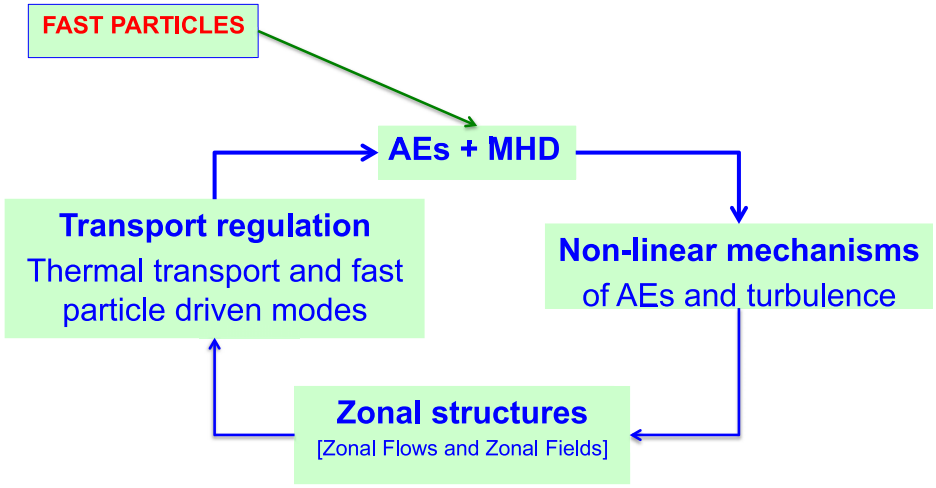

Figure 5. Possible interplay between fast particles driven modes and transport regulation via ZFs under investigation in the TJ-II stellarator.

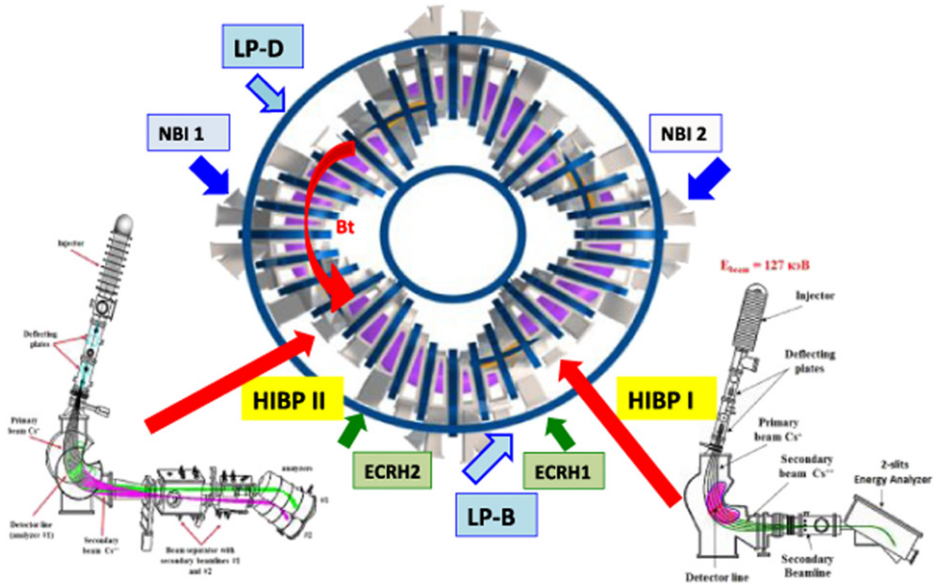

Figure 6. TJ-II plasmas are heated by ECRH (2 × 200 kW gyrotrons) and NBI (2 × 500 kW co—NBI-1- and counter—NBI-2). The dual HIBP system (HIBP-I and HIBP-2) was used to study the temporal and spatial evolution of density and plasma potential profiles, fluctuation levels and long-range-correlations (LRC) as proxy of ZFs in the plasma core region. The TJ-II stellarator is also equipped with a dual system of Langmuir-probe (LP) arrays placed at two different toroidal and poloidal locations: sector B (LP-B) and sector D (LP-D).

(shot 49598) with densities in the range $n \approx 0.50 \times 10^{19}$ m^{-3}. This sensitivity would reflect the influence of plasma location or/and the proximity of the electron–ion root transition on ZFs [37]. Figure 10 also shows that the amplitude of LRC reaches high values (coherence in the range of 0.8) at the transition to plasmas with Alfvénic instabilities.

Recently experiments aimed at obtaining the 2D distribution of plasma potential, density and their fluctuations have been performed in TJ-II using HIBP measurements [38].

In conclusion, LRCs have been unambiguously detected in the plasma core in ECRH and combined ECRH and NBI scenarios in the TJ-II stellarator. LRCs are observed in plasma potential fluctuations but not in density fluctuations as expected for ZF structures. These results, together with previous observations of edge ZFs in TJ-II, show that ZF structures are ubiquitous in the whole plasma cross-section in the TJ-II stellarator. In plasma scenarios with combined ECR and NBI heating, LRCs are detected both at the AE frequencies and at low frequencies (<10 kHz), with an amplitude that depends on the plasma scenario. It is an open question whether those ZFs can be directly driven by fast particle effects or/and are the consequence of the plasma scenario.

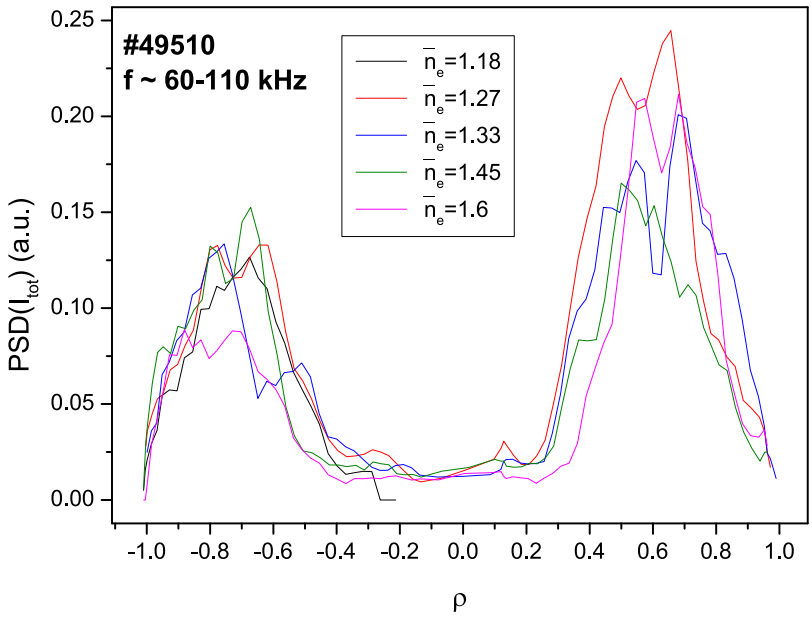

Figure 7. (*a*) Radial localization of AEs (shot 49510). The destabilization of several types of AEs (GAEs, HAEs and possibly TAEs) and energetic particle modes is predicted by the FAR3d code in TJ-II [21].

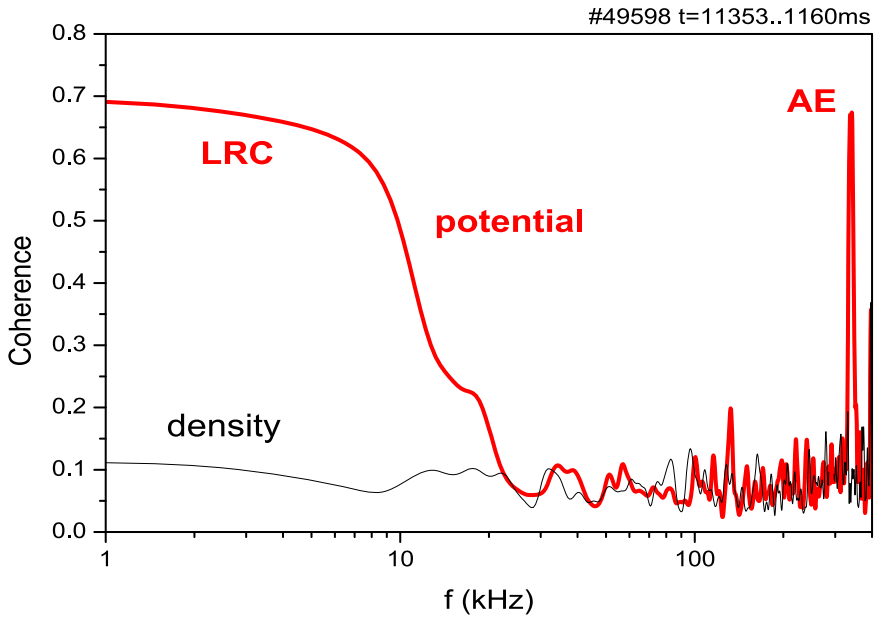

Figure 8. (Shot 49598) Frequency resolved LRC for density and potential fluctuations during the combined ECRH + NBI scenario.

4. Towards the characterization of the interaction between neoclassical and turbulent transport mechanisms

4.1. Turbulence spreading and radial electric fields

The SOL width is determined by competition between cross-field and parallel transport. It has recently been suggested that radial turbulence spreading may play an important role in setting the SOL width [39, 40] with important implications for ITER. Due to its flexibility to modify radial electric fields from positive to negative values in a continuous manner, stellarators are unique physics laboratories to validate models based on the influence of radial electric field (E_r) effects on turbulence spreading and edge-SOL coupling. The ambipolarity condition (i.e. the equality of ion and electron fluxes) determining the radial NC electric field has two stable roots: the ion root with typically negative E_r, usually achieved in high density plasmas, and the electron root with positive E_r, that is typically realized when electrons are subject to strong heating (ECRH) [37].

We have investigated the impact of E_r on turbulence propagation and the coupling between the plasma edge and the SOL during electron–ion root transitions where E_r is changed in a controlled manner from positive to negative values [41]. Plasma fluctuations are dominated by broadband turbulence

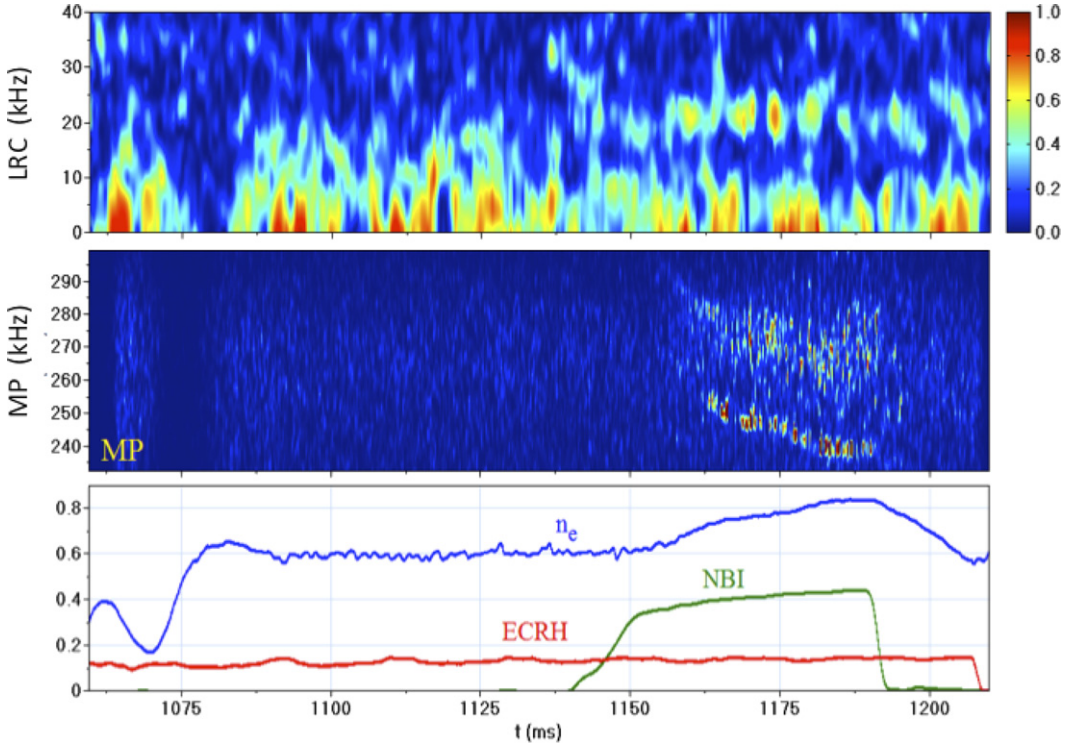

Figure 9. (Shot 49591) (Top) Time evolution of LRC measured in the plasma core ($\rho \approx 0.6$) during ECRH and NBI scenarios; (middle) spectrogram of high frequency magnetic fluctuations measured by magnetic probes (230–300 kHz) showing the appearance of specific AEs; (bottom) evolution of plasma density during ECRH to NBI scenarios. The plasma density was about $n \approx 0.60 \times 10^{19}$ m^{-3} in the pure ECRH scenario and $n \approx 0.6$–0.8×10^{19} m^{-3} in the combined ECRH + NBI scenario.

in ECRH scenarios which amplitude increases with heating power [42]. It is shown that E_r does not only affect the radial turbulence correlation length but is also capable of reducing the propagation of turbulence from the edge into the SOL. To do so, we make use of the transfer entropy (TE), a powerful statistical tool to follow the propagation of perturbations [43]. Thus, we found that the effective radial propagation from the edge to the SOL was very nearly blocked in the edge region in the ion root phase ($E_r < 0$) as compared to the electron root ($E_r > 0$) (figures 11 and 12). This is fully consistent with previous studies where E_r was actively modulated by edge biasing [44]. These observations are highly relevant for the understanding of the mechanisms that determine the SOL width. The radial electric field was also found to have a profound impact on turbulent intermittence [45]. This discovery opens up a new window for the study of the complex interactions between E_r and turbulence.

4.2. Edge zonal flows and radial electric fields

In stellarators, NC physics determines E_r at long length scales [46]. In addition, turbulent mechanisms (e.g. ZFs) can affect the E_r radial length scales. The unique experimental system that is the TJ-II stellarator has made it possible to obtain direct experimental evidence of self-organization processes consistent with the concept of ZFs. Recent experiments, developed within the framework of intense international collaborations, have demonstrated the influence of plasma ECRH and NBI heating conditions [47], the entangled role between turbulence and particle orbits [48], the influence of isotopic mass [49] and proximity to operational (density) limits [50] on the properties and dynamics [51] of ZFs in the TJ-II stellarator.

Figures 13 and 14 show the radial scale of LRCs in hydrogen and deuterium plasmas [49] and the radial modulation of dynamical radial electric fields due to edge ZFs in the plasma edge [47]. In NBI plasma scenarios, the radial size increases with isotope mass. The radial scale of LRC structures in NBI plasmas is about of 20 ion Larmor radii, comparable to the radial scale length of NC radial electric fields. Furthermore, results point towards the amplification of low frequency, coherent, global fluctuations with similar properties as ZFs in the vicinity of the density limit. Whether the threshold radiation value for the density limit as well as the conditions to reach stationary regimes would be partially affected by the amplitude of (fluctuating and DC) ZFs is an open question [50].

The interplay between NC radial electric fields, Reynolds stress gradients and LRCs has been investigated in different plasma scenarios in TJ-II. Turbulent driven acceleration alone cannot explain the dynamics of ZFs whose radial width is affected by the isotope mass [48]. These results are in line

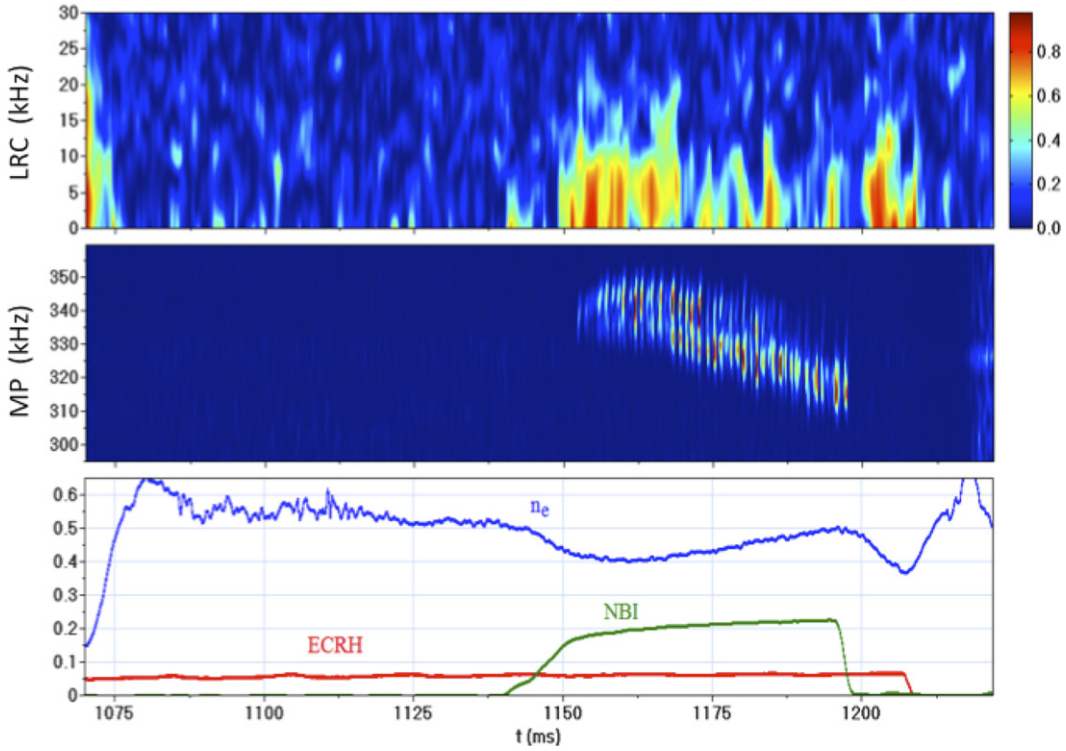

Figure 10. (Shot 49598) (Top) Time evolution of LRC measured in the plasma core ($\rho \approx 0.3$) during ECRH and NBI plasmas scenarios; (middle) spectrogram of high frequency fluctuations (300–350 kHz) showing the appearance of specific AE; (bottom) evolution of plasma density during ECRH and NBI scenarios. Plasma density was about $n \approx 0.50$–0.55×10^{19} m^{-3} in pure ECRH scenario and $n \approx 0.45$–0.50×10^{19} m^{-3} in the combined ECRH + NBI scenario.

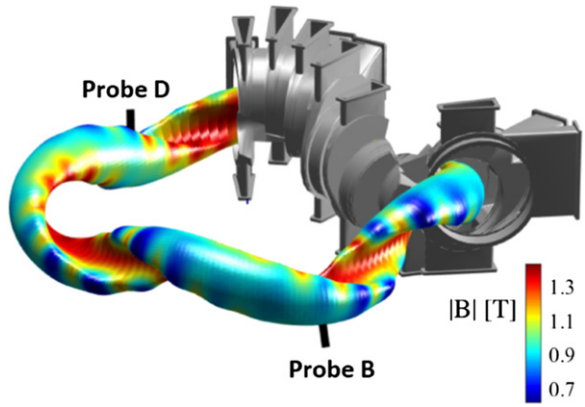

Figure 11. Dual edge probe array used to investigate the influence of edge radial electric fields in edge-SOL coupling (section 4.1) and the properties of edge ZFs (section 4.2).

with the expectation that the interplay between turbulent and NC mechanisms is an important ingredient of the dynamics of edge ZFs.

5. Power exhaust: liquid metals

Liquid metal-based divertors are at present promising alternatives to the use of solid elements for the power exhaust handling in a fusion reactor. Several aspects of the behaviour of liquid metals exposed to hot and cold plasmas in a capillary porous system (CPS) container were investigated at the LNF. These include:

(a) Solid and liquid samples of Li/LiSn/Sn in a CPS arrangement were exposed to the edge plasma in the TJ-II stellarator [52]. From the attenuation of the corresponding species (Li or Sn) and using a simple 1D model, the kinetic energy (E_k) of ejected atomic species was evaluated. The evolution of E_k with sample temperature deduced for Li atoms is well correlated with the different relative contributions of sputtered/evaporated atoms given by the thermal sputtering model. However, the recorded mean free paths for the ejected Sn atoms under sputtering conditions (low T) imply unrealistic high energies if the bibliographic data for the ionization rate constant of Sn are assumed.

(b) The retention of evaporated or plasma injected lithium on W at several temperatures was investigated in order to assess its impact on a fusion reactor operating with hot first wall. It was concluded [53] that an exponentially decaying retention as the first-wall temperature is increased takes place, with negligible D/Li ratios at $T > 350$ °C. On the other hand, D retention of liquid Sn and LiSn alloys was studied in DC glow discharges of D. Retention of H isotopes in the form of bubbles has been observed in liquid tin exposed to high D fluxes. This has been attributed to the low solubility and diffusivity of D into Sn. Droplet ejection of Sn upon bursting of such

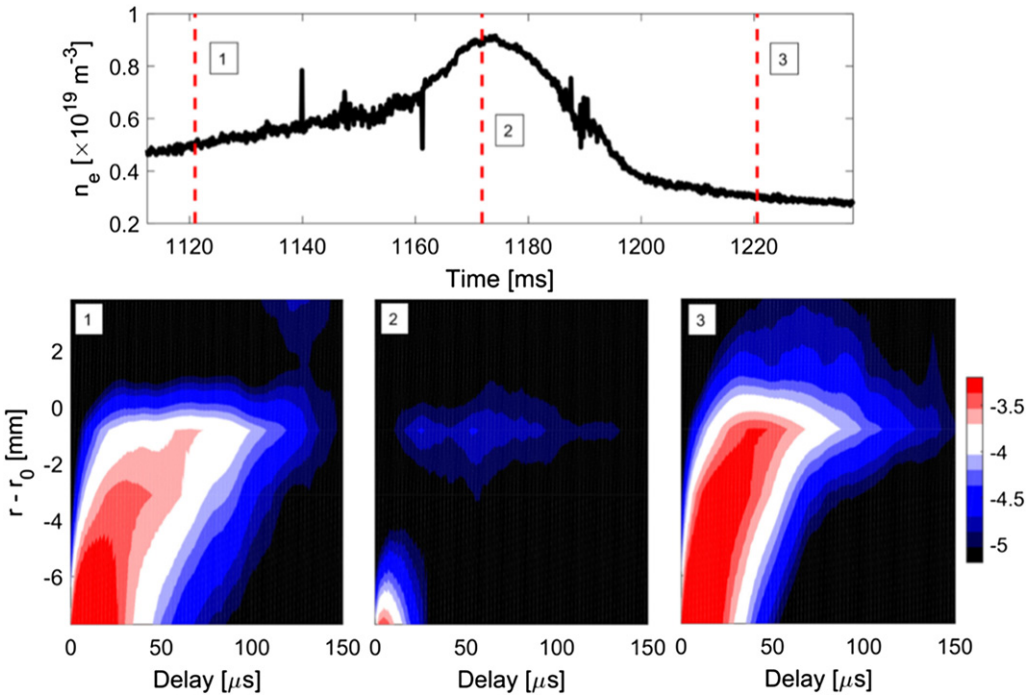

Figure 12. Radial propagation of plasma turbulence in the plasma edge: (1) electron root, (2) ion root, and (3) electron root with lower density. The edge E_r changes sign from positive (in the range of 2 kV m^{-1} at $\rho \approx 0.8$) to negative (in the range of -2 kV m^{-1} at $\rho \approx 0.8$) as the plasma makes a transition from the electron to the ion root at about $t \approx 1160$ ms. Radial propagation have been studied by taking the inner most pin of a rake Langmuir probe ($r - r_0 \approx -10$ mm), where r_0 is the position of the LCFS, as a reference and calculating the TE with all other pins aligned radially with a mutual separation of 2 mm. Reproduced courtesy of IAEA. Figure from [41]. © EURATOM 2019.

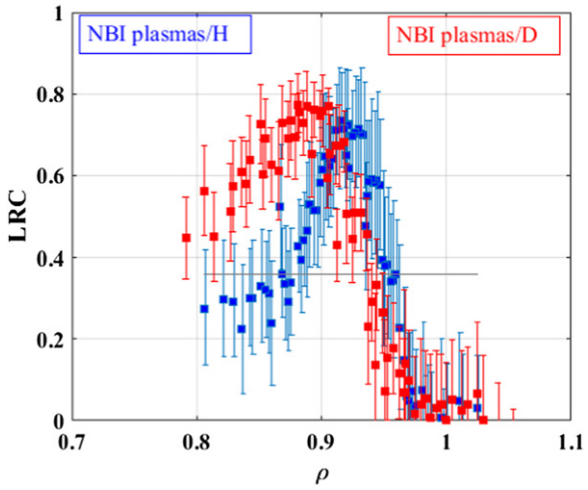

Figure 13. Radial profile of edge LRC in hydrogen and plasmas dominated by deuterium (≈70% D) in NBI scenarios. This result shows the first direct experimental evidence of ZFs width control by isotope mass [49].

bubbles may represent a strong source of plasma pollution, thus preventing its use in a fusion plasma reactor. No bubble formation was seen when liquid tin is exposed to these plasmas, in contradiction with recent observations [54, 55]. Furthermore, a much higher retention was deduced for LiSn alloys, and bubble formation right upon exposure to the D GD plasma was observed.

(c) Oblique magnetron sputtering and laser patterning were used to produce textured W surfaces. Their wetting by liquid lithium and further spreading by capillarity was seen to depend critically on some characteristic scale in the range of tens to hundred of microns [56]. The porous structures created by oblique magnetron sputtering may be sorted out in terms of some characteristic scales such as the filament spacing in both directions, the filament length and their ratios. At present is not possible to fully isolate their respective relevance for wetting but significant changes were seen during the scanning of those characteristic parameters.

(d) Secondary electron emission of liquid Li surfaces in a CPS arrangement was investigated for the first time. Even at base pressures in the range of 10^{-7} mbar, oxidation of Li by residual water and oxygen takes place, leading to an increase in the SEE yield by a factor of 4 compared to the pristine surface. However, it was found that a fast annealing of the Li sample at 450–500 °C was enough to revert the values to those corresponding to clean surfaces [57]. It is speculated that diffusion of superficial lithium oxide into the bulk, together with enhanced solubility, is behind the observations, thus providing a practical way to characterize and condition lithium surfaces exposed to a hot plasma.

(e) The OLMAT facility, aimed at testing LM prototypes under DEMO-relevant heat loads [58] was constructed and installed (figure 15). It is based on the use of the

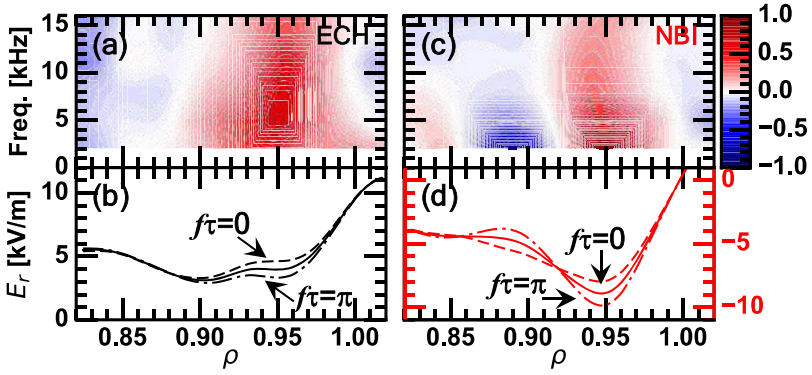

Figure 14. Radial structure of edge zonal structures in plasmas maintained with heating systems at the resonant cyclotron frequency of electrons (ECRH; (*a*)/(*b*)) and with neutral beam heating (NBI; (*c*)/(*d*)) in the TJ-II stellarator. The width of ZF structures narrows when transitioning from ECRH plasmas to NBI plasmas. Radial coherence of the waveforms of the low frequency global oscillation of the radial electric field has been measured using radial rake probes. Reproduced courtesy of IAEA. Figure from [47]. Copyright (2019) IAEA.

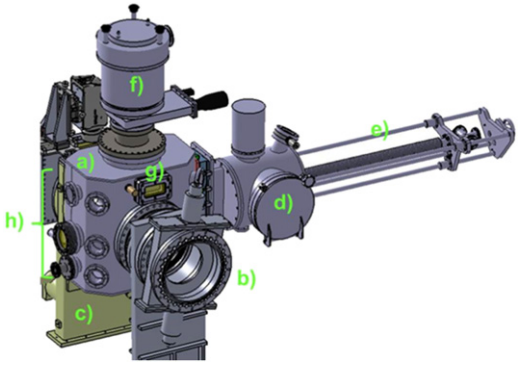

Figure 15. CAD design of OLMAT. (*a*) irradiation chamber; (*b*) valve to NBI; (*c*) valve to TJ-II; (*d*) pre-chamber for sample loading; (*e*) sample insertion system; (*f*) upper turbopump with liquid metal condensation bafflers; (*g*) BaF2 optical window for infrared thermography; (*h*) diagnostic ports and windows.

neutral beams (NBI) of the TJ-II stellarator for the irradiation of LM targets (mainly CPS) at DEMO-relevant powers. The characteristics of the NBI beam are adequate for the simulation of steady state and slow transient powers (10–20 MW m^{-2}) including vapour shielding and fatigue studies. Moreover, the NBI beam is wide enough to irradiate large samples (<20 cm diameter), allowing redeposition studies of the eroded and evaporated material. In a second stage of the project a Q-CW, high-power fibre laser will be used to simulate ELM-like powers in a small area, or the strike point power deposition profile.

6. Conclusions

The TJ-II team has exploited the outstanding configurational flexibility of the device and its set of advanced and unique diagnostics to provide experimental results in some key fusion research areas. Our reinforced capabilities in theory and modelling have allowed comparison and validation activities with regard to NC and turbulent mechanisms. The results described here demonstrate our improved physics understanding of phenomena in impurity transport, plasma fuelling physics, AE control and stability, the intertwinement of turbulent and NC mechanisms and plasma exhaust that complements the empirical approach, with the following main conclusions:

- *Asymmetries.* The validation of a variation of the radial electric field on the flux surface (i.e. poloidal asymmetries) has been successfully accomplished and its dependence with the magnetic configuration investigated. Poloidal asymmetries in radial electric field are found, that depend on the plasma collisionality, consistent with NC simulations. Poloidal asymmetries in the amplitude of the wave number spectrum are consistent with a spatial localization of instabilities, as found in GK simulations.
- *Fuelling physics and impurities.* Research on the physics and modelling of plasma core fuelling with pellet and TESPEL injection has shown that, although post-injection particle radial redistributions can be understood qualitatively from NC mechanisms, turbulence and fluctuations are strongly affected during the ablation process. Enhanced pellet ablation due to fast-electron, as well as interactions between outward drifting pellet material and resonant surfaces that can lead to the abrupt deceleration of the pellet cloud, have been reported. Density fluctuations appear both at the positive and negative density gradient regions, being stronger in the negative gradient region.
- *Edge—SOL coupling.* Advanced analysis tools based on TE have shown that radial electric field does not only affects the radial turbulence correlation length but it is also capable of reducing the propagation of turbulence from the edge into the SOL.
- *Zonal structures in the edge and the core regions.* Direct experimental observation of long range correlated structures (LRC) shows that ZFs are ubiquitous in the whole plasma cross-section in the TJ-II stellarator. The radial width of the LRC is affected by plasma heating and ion mass.
- *Fast particle physics.* Alfvénic activity control strategies using ECRH and ECCD as well as the relation between zonal structures and AEs are reported. Although so far

no causal relationship could be established between the amplitude of ZFs and AEs, TJ-II experiments paves the way to study the role of fast particles in the driving or/and damping of ZFs.

- *Liquid metals and power exhaust.* The behaviour of liquid metals exposed to hot and cold plasmas in a CPS container were investigated. Kinetic energies, D content, wetting and SEE properties were characterized. A new facility, OLMAT, has been constructed for testing LM target prototypes under DEMO-relevant heat loads.

Acknowledgments

This work has been carried out within the framework of the EUROfusion Consortium and has received funding from the Euratom research and training programme 2014–2018 and 2019–2020 under Grant Agreement No. 633053. The views and opinions expressed herein do not necessarily reflect those of the European Commission. It has been partially funded by the Ministerio de Ciencia e Inovación of Spain under projects FIS2017-89326-R and PGC2018-097279-B-I00. The research done by Kurchatov team supported by Russian Science Foundation, Project 19-12-00312. FP thanks the ERASMUS+ programme for the opportunity to perform this research while visiting Ciemat. AVM was partly supported by the Competitiveness Program of NRNU MEPhI. MEK gratefully acknowledges partial support from US DOE Grant DE-SC0020269.

References

[1] Estrada T. *et al* 2019 Turbulence and perpendicular plasma flow asymmetries measured at TJ-II plasmas *Nucl. Fusion* **59** 076021
[2] Sánchez E., Estrada T., Velasco J.L., Calvo I., Cappa A., Alonso A., García-Regaña J.M., Kleiber R. and Riemann J. 2019 Validation of global gyrokinetic simulations in stellarator configurations *Nucl. Fusion* **59** 076029
[3] Pedrosa M.A., Alonso J.A., García-Regaña J.M., Hidalgo C., Velasco J.L., Calvo I., Kleiber R., Silva C. and Helander P. 2015 Electrostatic potential variations along flux surfaces in stellarators *Nucl. Fusion* **55** 052001
[4] García-Regaña J.M. *et al* 2018 On-surface potential and radial electric field variations in electron root stellarator plasmas *Plasma Phys. Control. Fusion* **60** 104002
[5] Sánchez E. *et al* 2021 Gyrokinetic simulations in stellarators using different computational domains *28th IAEA-2021*
[6] Barnes M., Parra F.I. and Landreman M. 2019 Stella: an operator-split, implicit-explicit δf-gyrokinetic code for general magnetic field configurations *J. Comput. Phys.* **391** 365
[7] García-Regaña J.M. *et al* 2021 Turbulent impurity transport simulations in Wendelstein 7-X plasmas *J. Plasma Phys.* **87** 855870103
[8] Calvo I., Velasco J.L., Parra F.I., Alonso J.A. and García-Regaña J.M. 2018 Electrostatic potential variations on stellarator magnetic surfaces in low collisionality regimes *J. Plasma Phys.* **84** 905840407
[9] Velasco J.L., Calvo I., Parra F.I., d'Herbemont V., Smith H.M., Carralero D. and Estrada T. 2021 Fast simulations for large aspect ratio stellarators with the neoclassical code KNOSOS *Nucl. Fusion* **61** 11603
[10] Velasco J.L., Calvo I., Parra F.I. and García-Regaña J.M. 2020 KNOSOS: a fast orbit-averaging neoclassical code for stellarator geometry *J. Comput. Phys.* **418** 109512
[11] Carralero D. *et al* 2020 Characterization of the radial electric field and edge velocity shear in Wendelstein 7-X *Nucl. Fusion* **60** 10601
[12] Estrada T. *et al* 2021 *Nucl. Fusion* **61** 046008
[13] Spong D.A. *et al* 2001 Physics issues of compact drift optimized stellarators *Nucl. Fusion* **41** 711–6
[14] Mccarthy K.J. *et al* 2017 Plasma fuelling with cryogenic pellets in the stellarator TJ-II *Nucl. Fusion* **57** 056039
[15] Panadero N. *et al* 2018 Experimental studies and simulations of hydrogen pellet ablation in the stellarator TJ-II *Nucl. Fusion* **58** 026025
[16] Mccarthy K.J. *et al* 2017 Comparison of cryogenic (hydrogen) and TESPEL (polystyrene) pellet particle deposition in a magnetically confined plasma *Europhys. Lett.* **120** 25001
[17] Mccarthy K.J. *et al* 2019 The impact of fast electrons on pellet injection in the stellarator TJ-II *Plasma Phys. Control. Fusion* **61** 014013
[18] Mccarthy K.J. *et al* 2021 *Nucl. Fusion* **61** 076014
[19] Sharma R. *et al* 2020 Measurements of 2D poloidal plasma profiles and fluctuations in ECRH plasmas using the heavy ion beam probe system in the TJ-II stellarator *Phys. Plasmas* **27** 062502
[20] Varela J., Nagasaki K., Nagaoka K., Yamamoto S., Watanabe K.Y., Spong D.A., Garcia L., Cappa A. and Azegami A. 2020 Modeling of the ECCD injection effect on the Heliotron J and LHD plasma stability *Nucl. Fusion* **60** 112015
[21] Cappa Á. *et al* 2021 *Nucl. Fusion* **61** 066019
[22] Mulas S. *et al* 2021 Experimental validation of neutral beam current drive simulations in TJ-II plasmas *IAEA 2021, TH/850*
[23] Ascasibar E. *et al* 2021 Measurements of magnetic fluctuations in TJ-II plasmas with new in-vessel helical arrays of magnetic coils *Rev. Sci. Instrum.* (to be submitted)
[24] Citrin J. *et al* 2013 Nonlinear stabilization of tokamak microturbulence by fast ions *Phys. Rev. Lett.* **111** 155001
[25] Mantica P. *et al* 2011 A key to improved ion core confinement in the JET tokamak: ion stiffness mitigation due to combined plasma rotation and low magnetic shear *Phys. Rev. Lett.* **107** 135004
[26] Di Siena A., Görler T., Doerk H., Poli E. and Bilato R. 2018 Fast-ion stabilization of tokamak plasma turbulence *Nucl. Fusion* **58** 054002
[27] Mazzi S. *et al* 2020 *Nucl. Fusion* **60** 046026
[28] Chen L. and Zonca F. 2012 Nonlinear excitations of zonal structures by toroidal Alfvén eigenmodes *Phys. Rev. Lett.* **109** 145002
[29] Qiu Z., Chen L., Zonca F. and Chen W. 2019 Nonlinear excitation of a geodesic acoustic mode by toroidal Alfvén eigenmodes and the impact on plasma performance *Nucl. Fusion* **59** 066031
[30] Di Siena A., Görler T., Poli E., Navarro A.B., Biancalani A. and Jenko F. 2019 Electromagnetic turbulence suppression by energetic particle driven modes *Nucl. Fusion* **59** 124001
[31] Melnikov A.V. *et al* 2017 Heavy ion beam probing-diagnostics to study potential and turbulence in toroidal plasmas *Nucl. Fusion* **57** 072004
[32] Melnikov A.V. *et al* 2010 Internal measurements of Alfvén eigenmodes with heavy ion beam probing in toroidal plasmas *Nucl. Fusion* **50** 084023
[33] Nagaoka K. *et al* 2013 Mitigation of NBI-driven Alfvén eigenmodes by electron cyclotron heating in the TJ-II stellarator *Nucl. Fusion* **53** 072004
[34] Melnikov A.V. *et al* 2014 Effect of magnetic configuration on frequency of NBI-driven Alfvén modes in TJ-II *Nucl. Fusion* **54** 123002

[35] Pedrosa M.A., Silva C., Hidalgo C., Carreras B.A., Orozco R.O. and Carralero D. 2008 Evidence of long-distance correlation of fluctuations during edge transitions to improved-confinement regimes in the TJ-II stellarator *Phys. Rev. Lett.* **100** 215003
[36] Melnikov A.V. *et al* 2011 Plasma potential and turbulence dynamics in toroidal devices (survey of T-10 and TJ-II experiments) *Nucl. Fusion* **51** 083043
[37] Velasco J.L., Alonso J.A., Calvo I. and Arévalo J. 2012 Vanishing neoclassical viscosity and physics of the shear layer in stellarators *Phys. Rev. Lett.* **109** 135003
[38] Melnikov A. Submitted to *Plamsa Phys. Control. Fusion*
[39] Chang C.S. *et al* 2017 Gyrokinetic projection of the divertor heat-flux width from present tokamaks to ITER *Nucl. Fusion* **57** 116023
[40] Chen B. *et al* 2018 Progress towards modeling tokamak boundary plasma turbulence and understanding its role in setting divertor heat flux widths *Phys. Plasmas* **25** 055905
[41] Grenfell G., van Milligen B.P., Estrada T., Liu B., Silva C., Spolaore M. and Hidalgo C. 2020 The impact of edge radial electric fields on edge-scrape-off layer coupling in the TJ-II stellarator *Nucl. Fusion* **60** 014001
[42] Voldiner I., van Milligen B., Hidalgo C. and Sanchez R. 2021 Rapid response of turbulence to ECRH power modulation in the TJ-II stellarator 47th EPS Conference on Plasma Physics, ECA **Vol. 45A** P2.1052
[43] Van Milligen B., Carreras B., García L. and Nicolau J. 2019 The radial propagation of heat in strongly driven non-equilibrium fusion plasmas *Entropy* **21** 148
[44] Grenfell G., Van Milligen B.P., Losada U., Ting W., Liu B., Silva C., Spolaore M. and Hidalgo C. 2019 Measurement and control of turbulence spreading in the scrape-off layer of TJ-II stellarator *Nucl. Fusion* **59** 016018
[45] Van Milligen B.P., Carreras B.A., García L. and Hidalgo C. (the TJ-II team) 2020 The localization of low order rational surfaces based on the intermittence parameter in the TJ-II stellarator *Nucl. Fusion* **60** 056010
[46] Helander P. and Simakov A.N. 2008 Intrinsic ambipolarity and rotation in stellarators *Phys. Rev. Lett.* **101** 145003
[47] Kobayashi T., Losada U., Liu B., Estrada T., van Milligen B.P., Gerrú R., Sasaki M. and Hidalgo C. 2019 Frequency and plasma condition dependent spatial structure of low frequency global potential oscillations in the TJ-II stellarator *Nucl. Fusion* **59** 044006
[48] Gerrú R., Mulas S., Losada U., Castejón F., Liu B., Estrada T., van Milligen B.P. and Hidalgo C. 2019 On the interplay between turbulent forces and neoclassical particle losses in zonal flow dynamics *Nucl. Fusion* **59** 106054
[49] Losada U. *et al* 2021 Spatial characterization of edge zonal flows in the TJ-II stellarator: the roles of plasma heating and isotope mass *Plasma Phys. Control. Fusion* **63** 044002
[50] Fernández-Ruiz D. *et al* 2021 On the evolution of zonal flows in the proximity of the density limit in the TJ-II stellarator *Nucl. Fusion* **61** 126038
[51] Alonso J.A. *et al* 2017 Observation of oscillatory radial electric field relaxation in a helical plasma *Phys. Rev. Lett.* **118** 185002
[52] Tabarés F.L. *et al* 2018 Generation and transport of atomic lithium during the exposure of liquid metals to hot plasmas in TJ-II *Nucl. Mater. Energy* **17** 314
[53] De Castro A., Sepetys A., González M. and Tabarés F.L. 2018 Temperature dependence of liquid lithium film formation and deuterium retention on hot W samples studied by LID-QMS. Implications for future fusion reactors *Nucl. Fusion* **58** 046003
[54] Ou W., Al R.S., Vernimmen J.W.M., Brons S., Rindt P. and Morgan T.W. 2020 Deuterium retention in Sn-filled samples exposed to fusion-relevant flux plasmas *Nucl. Fusion* **60** 026008
[55] Manhard A., Schwarz-Selinger T., Balden M., Dürbeck T., Maier H. and Neu R. 2020 Deuterium retention in solid and liquid tin after low-temperature plasma exposure *Nucl. Fusion* **60** 106007
[56] Muñoz-Piña S. *et al* 2020 Wetting and spreading of liquid lithium onto nanocolumnar tungsten coatings tailored through the topography of stainless steel substrates *Nucl. Fusion* **60** 126033
[57] Oyarzabal E. and Tabarés F.L. 2021 Strongly temperature-dependent, anomalous secondary electron emission of liquid lithium surfaces exposed to a plasma *Nucl. Mater. Energy* **27** 100966
[58] Alegre D., Oyarzabal E., Tafalla D., Liniers M., Soleto A. and Tabarés F.L. 2020 Design and testing of advanced liquid metal targets for DEMO divertor: the OLMAT project *J. Fusion Energy* **39** 411